Comparison between an Object-Oriented Model and a Fast Fourier Transform Model for Gravitational Wave Interferometers

Erika D'Ambrosio

Ligo Laboratory, California Institute of Technology, Pasadena CA91125

(June 2^{nd}, 2001)

The features of two completely different numerical approaches will be reviewed. Such features are closely linked with the specific kind of issue that is to be analysed using one of the two approaches. The motivation for doing a comparison is checking on the reliability of the two codes for simulating realistic cases both the programs can deal with. This was essential to find out the reasons for discrepancies and fix bugs.

After preliminary analyses, diagnostics and improvements brought to a very good agreement between the models, within few percents even for severe perturbations and such an agreement can be further reduced at CPU time expenses whenever the specific problem to be addressed is worthwhile. Runs have been made for testing both the carrier field which resonates in the arms and in the recycling cavity, and its sidebands that only resonate in the recycling cavity. The sidebands are particularly interesting for certain perturbations are not compensated by some adjustments of the lengths of the cavities and as a result they show different behaviours. This asymmetry has been detected in real measurements and numerical valid tools are essential to develop models for explaining the optical effects.

INTRODUCTION

In Sec.I the main differences between the modal model and the FFT model will be reviewed in order to understand which perturbations can be managed by both the numerical programs. For example in the FFT scheme the maps of imperfections are put on the top of mirrors' spherical surfaces and those are kept fixed for the entire run, while in the modal model both the field and mirror are distorted by their reciprocal interaction. This makes the former the right tool for studying tolerance limits on the mirrors' imperfections requirements and the latter for simulating non-linear effects related with the light power. For instance in the modal model input files a lot of informations are needed such as specific heat, thermal conductivity, refractive index and its dependance on temperature and so on. Also there are significant differences in the definition of mirrors' losses and in general the starting parameters must be very carefully evaluated with a view to use the two different tools for achieving the same goal. This is due to the completely different representations of the electric field; an array of TEM modes weighted by different coefficients in the modal model and a grid for the transverse section in the FFT code. In Sec.II the results obtained by using the two simulation schemes are compared for situations they both can deal with. The most important outcome of this validation is that the numerical procedure that has been worked out for the modal model to generate the effects of geometrical cold perturbations, has been also implemented as routine for evaluating thermal distortions when dynamical tranformations are allowed. In other words even if a comparison between the different tools has been limited to static deformations, those tests have been useful to improve an algorithm that works for simulating dynamical interactions as well.

I. COMPARISON OF THE MODAL MODEL AND THE FFT MODEL WORKING PRINCIPLES AND THE INFORMATIONS THEY NEED

The FFT-code and the Melody program are two simulation tools for gravitational wave detectors like LIGO.

The aims they were written for are completely different; the former was planned to investigate requirements and tolerances for all the mirrors used inside the interferometer and the latter is pretty focused on the perturbations caused by thermal effects on both mirrors and beam. In the FFT-code measured or simulated maps may be introduced instead of ideal spherical mirrors, so that realistic or hypotetical interesting situations may be studied when analytical calculations are not easy to pursue. On the contrary in the Melody simulation the program is in charge of modifying the shape of the mirrors that are not fixed by the user.

There are many situations though that can be approached with both the programs.

Before illustrating some simple cases I am giving an outline of the parameters that are needed by the two programs to start. Many of them are straight and are shown in Table I. Others are typical of only one of them such as the spot size and radius of curvature of the beam on the ITM on-line mirror in the FFT-code. The input file for the FFT-code is one, while there are several files to give the system's constants if Melody is run. One of those files regards the informations on materials such as conductivity, thermal expansion and so on and three files contain the specifics of the two arm cavities and the central part.

Also the way the two codes follow is rather different. For the FFT the paraxial approximation is used in order to calculate the propagation between mirrors, as a matrix operator in the spatial frequency domain. The lengths are optimized in order to achieve a stationary locked configuration and the power stored inside the arms and the recycling cavity is evaluated. The total power may be analysed for checking purposes using the main modes decomposition TEM00, TEM10 and TEM01 in order to realize for example possible asymmetries due to mirrors' tilt that can be simulated by the FFT-code. The Melody program

starts with a fixed number of modes that propagate back and forth between mirrors and the thermal effects are perturbatively evaluated at every iteration until stationarity is achieved.

Since those effects depend on the laser power, the energy level is increased at each step of a series starting from a low value to the one under investigation.

In the output files the power for every mode is displayed both for carrier and sidebands. The main features are recorded for every power cycle level and since the procedure is perturbative, the final configuration for each step represents the starting point for the next one. Some subtle differences in the terminology are worth noting; first the recycling cavity power is measured at the symmetric beamsplitter port while the FFT-code picks up the values both at the recycling mirror reflective side and at the bright port of the beamsplitter. Moreover the gain values for the FFT-code are just the power values normalized by the laser power which only represents a scale factor. On the contrary for the Melody code the power is a real variable that affects the physical behaviour of the system and the quantity named enhancement refers to the TEM00 mode only, normalized by the laser power. In the FFT-code the carrier and the sidebands are simulated by two different consecutive runs so that the cavities' lengths are optimized for the carrier and the Schnupp asymmetry is optimized for the sidebands. The power is shared by carrier and sidebands in Melody which treats the field as a whole.

The main informations are roughly collected in Tab.II. There are many output files for both the codes that can be looked at if some specific problem is to be addressed.

For example, the maps of the beam's cross-section obtained for some interesting pick-up points inside the interferometer may be analysed in some details using dedicated utilities for the FFT-code output grids. Also there are several files showing partial results that are especially useful for diagnostic purposes. The Melody output files include informations on the thermal distortion of the beam.

Indeed the final beam has a different composition in terms of a TEM basis than it initially had before the perturbative iterations. The mirrors' displacements and the final thermal focal lengths are also evaluated. Since all those thermal deformations are not allowed by the

FFT-code, the thermal perturbations must be disabled in the Melody program in order to make a comparison between the final values of the most important physical quantities. One simple case to start with may be a completely symmetric configuration with ideal spherical mirrors. Since this problem can be solved analytically too, the numerical results are supposed to be the same and equal to the mathematical predictions for both the programs.

II. SIMULATIONS OF SIMPLE IDEAL CASES AND COMPLEX REALISTIC PERTURBATIONS BOTH FOR THE CARRIER FIELD AND ITS SIDEBANDS

A. Variations of the reflectivity parameters and the cavities lengths

The first test has been the ideal interferometer, where the radius of curvature of the circulating field and the one of every mirror it impinges on match. This step was necessary in order to check the right informations have been provided in the input files.

The agreement with analytical calculations is within 0.06% for the FFT-code and 0.16% for Melody. Those values were obtained for $1W$ input power but if a $0.1W$ level is used the Melody results and the evaluations agree within 0.01% since the power is not simply a scale factor as it is in the FFT-code.

The next step has been to switch off one of the two arms. As a result the field promptly reflected back from the anti-reflective side of the mirror has a sign opposite to the one it would have got if it had gone into the arm through that mirror and been reflected. Both the codes implicitly assume resonant conditions in the two arms and cope with that change in sign by adding π to the phase.

This results from adjusting the position of the mirror by $\frac{\lambda}{4}$. It is interesting to note that if such adjustment is not included in mathematical calculations, the two ports of the beamsplitter are exactly swapped if compared with analytical predictions. This is a general feature for a Fabry-Perot cavity that is the reflected field's amplitude depends on how strongly it is rejected in anti-resonant conditions gaining a factor -1, or how tightly it

is locked in resonant conditions gaining a factor +1, because of the combination of the reflectivities of the end mirrors. This is important for example when the laser is modulated, generating sidebands which are anti-resonating in the arms of the interferometer. Such an effect is achieved with a macroscopic constraint on the length of the cavities:

$$\frac{2\pi\nu_{mod}}{c}2L = (2k+1)\pi \rightarrow \frac{2L\nu_{mod}}{c} = k + \frac{1}{2} = 639.500$$

where L is the length of the arm, ν_{mod} is the modulation frequency and k an integer value,

$$\frac{2\pi\nu_{mod}}{c}2L_{r.c.} = (2h+1)\pi \rightarrow \frac{2L_{r.c.}\nu_{mod}}{c} = h + \frac{1}{2} = 1.50000$$

with $L_{r.c.}$ the recycling cavity length and h any integer. Because of the different coupling with the arm for the carrier and the sidebands, the resonant conditions in the recycling cavity are different in the two cases. Respectively

$$\frac{2\pi\nu}{c}2L_{r.c.} = 2n\pi \qquad \frac{2\pi(\nu \pm \nu_{mod})}{c}2L_{r.c.} = (2m+1)\pi$$

where ν is the carrier frequency and n and m two any integers. When the arm is switched off

$$\frac{2\pi\nu}{c}2L_{r.c.} = (2n+1)\pi$$

becomes the resonant condition for the carrier inside the recycling cavity. The macroscopic constraint on the length of that cavity causes the sidebands to be anti-resonant. The only way to make the sidebands resonate inside the recycling cavity when the arms are switched off is to offset its length in order to have

$$\frac{2\pi\nu}{c}2L_{r.c.} = 2n\pi \qquad .$$

This trick works and it's useful to model the situation of misaligned external mirrors when the light going into the arms is completely lost. For experimental reasons related to the procedure for locking the interferometer, this is a very interesting case to model.

Next the effects of geometrical perturbations of the mirrors are addressed and discussed; the case of a smaller mirror and a decreased radius of curvature are simulated using the two approaches. After many tests and diagnostic studies the final results are shown.

B. Acting upon the diameter of one mirror and the radius of curvature

The numerical results have been compared with mathematical predictions for the cases described in Tab.III and Tab.V. Analytical approaches are not pursuable for the tests we are describing next. In Fig.1 the power stored in one arm is reported versus the diameter of the external mirror.

This test has been very useful because a major problem was affecting the modal model; the pseudolocker routine was pursuing a too good optimization cancelling the effects of the perturbation. Even turning that option off for perturbations up to $2cm$ the curve was flat. Moreover the asymmetry between the two arms due to this perturbation was not sensed at the dark port of the beamsplitter whose exit power was staying fixed at the low value corresponding to the unperturbed configuration. The kind of tests which have been made along are for example the check of the lengths chosen by the numerical locking procedure to look for the location of the power peaks around those values. Because of the high Finesse of the Fabry-Perot cavities the introduced offsets should be of few nanometers. In Fig.2 an example of such investigations is shown. When the codes are run the distances between mirrors are chosen in such a way that the round-trip phase of the carrier field is close to zero. Any slight perturbation can modify those distances from the ideal values defined in the equations above. Since the macroscopic lengths have beed designed in order to make the sidebands resonate inside the recycling cavity and anti-resonate in the arms, small adjustments of the initial values can easily bring the system out of such conditions. Both the simulation programs allow for the modulation frequency to be optimized in such a way that those changes are compensated. The idea is to maximize the recycling cavity gain, that corresponds to have the sideband fields not resonating at all in the arm cavities.

Indeed as they approach the exact anti-resonant condition, larger is the effect of rejection toward the recycling cavity increasing the power stored there. The curve shown in Fig.3 assumes exact anti-resonance in the arms. It is obtained using the parameters corresponding to the results of Tab.IV.

Because of the high reflectivity of the external mirror of the arms, the result of exact anti-resonance for the sidebands is equivalent to complete reflection back into the recycling cavity. Another feature characterizing the sidebands is their sensitivity to macroscopic displacement of the beamsplitter, necessary in real life for picking up the sideband signal at the asymmetric port and detect its quadrature with the carrier field according to a demodulation scheme. Since the phase variation induced by a gravitational wave is very small, this kind of detection allows a measurement in the first order of magnitude for the carrier field exiting the dark port. In Fig.4 the D.C. power measured at the dark port is shown as a function of the displacement of the beamsplitter. There are two symmetric peaks whose height is increased when the recycling cavity is "hermetic" for the sidebands.

If the recycling cavity doesn't behave as it were isolated, the peaks are moved toward larger values of the beamsplitter displacement and become broadened. The presence of some perturbations severely disrupts this simple picture. Comparing the results obtained by the modal model and the FFT method, when the modulation of the laser field is allowed, requires big control over a lot of phenomena and parameter changes. In order to keep things as simple as possible the modulation frequency has been kept fixed and only microscopic adjustments in the position of the beamsplitter were permitted. In Fig.5 the power stored in the recycling cavity is shown for smaller values of the radius of curvature of one internal mirror than "ideal".

This test is demanding since the recycling cavity becomes unstable. The carrier field results for the two codes show a very close agreement and decreasing the array size in the modal model only affects the sidebands data. Indeed using few modes gives a large discrepancy especially in the critical area of instability.

In order to disentangle the two problems of an imbalance between the sidebands and the overall gain largely reduced, the same perturbation has been applied to both the internal mirrors.

Both the two simulating codes have given the same data for the upper and lower sidebands. No optimization of the modulation frequency was allowed for this set of run nor

macroscopic variations of the beamplitter position. When the mirrors are largely perturbed the agreement between the data obtained by the different approaches is not satisfactory.

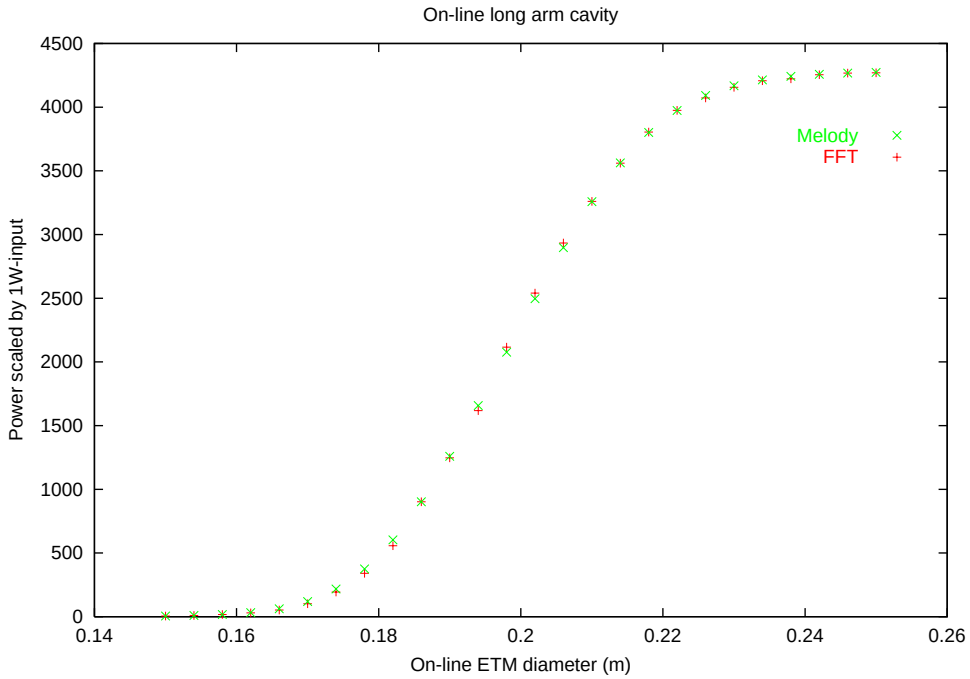

FIG. 1. The power built up in the Fabry-Perot cavity when the diameter of the external mirror is shortened. The results obtained by the two approaches agree within few percent.

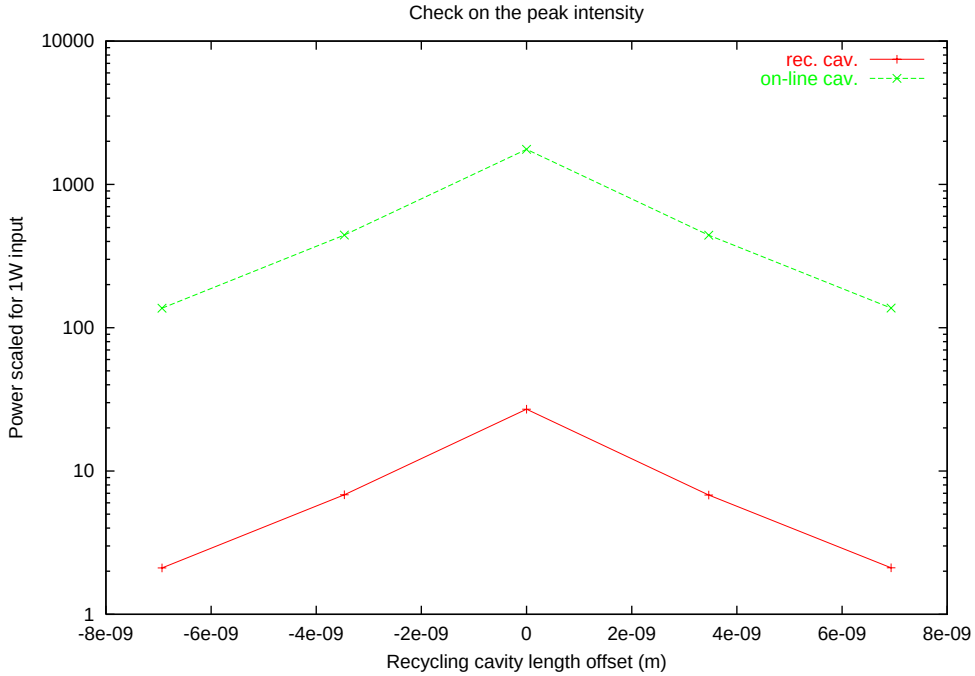

FIG. 2. The power gain is shown versus an offset taken around the value established at the end of the iterative procedure that looks for the resonance of the carrier field.

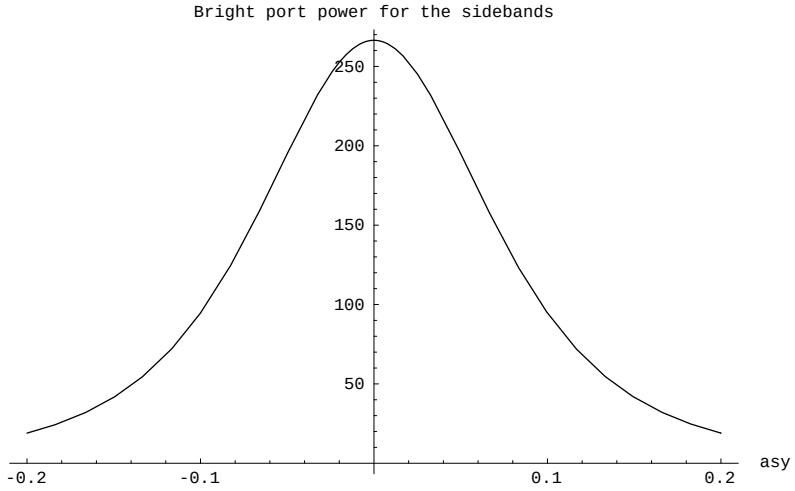

FIG. 3. The amount of sidebands' power circulating inside the recycling cavity depends on the leakage toward the arms and through the beamplitter dark port. The former factor affects the height of the central peak along the y-axis while the beamplitter's position changes the amount of light which is actually recycled; it clearly diminishes out of the symmetric position along the x-axis

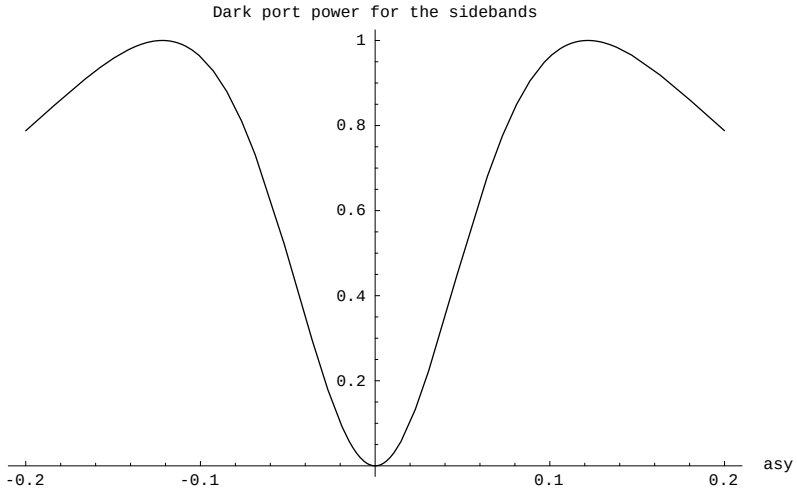

FIG. 4. The D.C. power at the dark port of the beamsplitter is shown as a function of the differential distance between that and the two long cavities. The numerical results are in agreement with this theoretical prediction within 0.1%. The maximum of this curve corresponds to an asymmetry of $12.18cm$ and it may vary according to the effective transmittivities of mirrors at the ends of the recycling cavity.

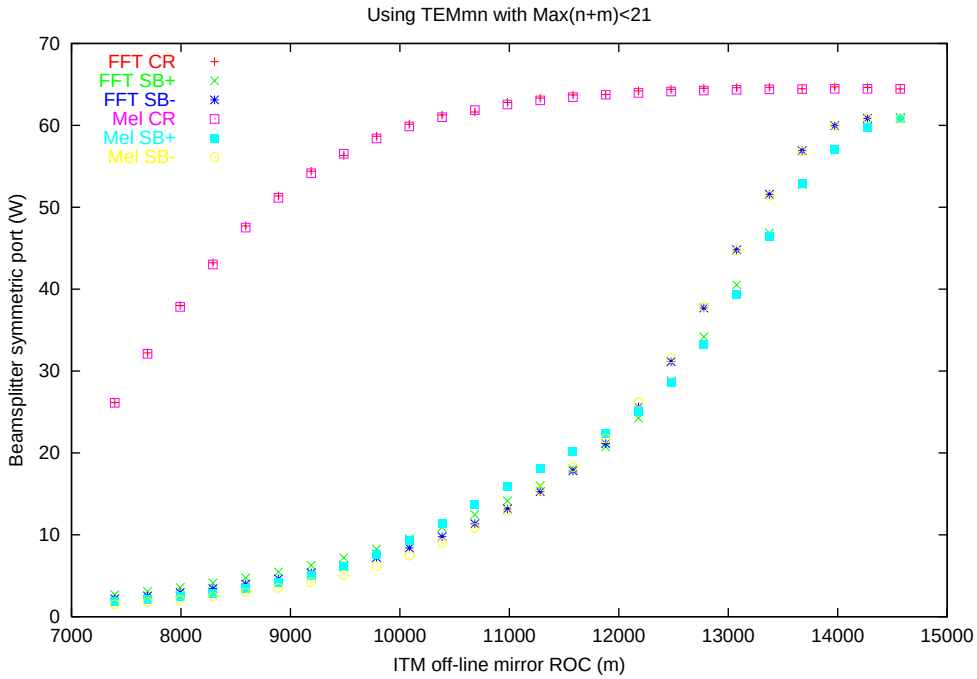

FIG. 5. The intensity of the light going through the symmetric port of the beamsplitter and recycled is shown for different radii of curvature of one internal mirror. The agreement is not as good when the size of the array in the modal model is smaller.

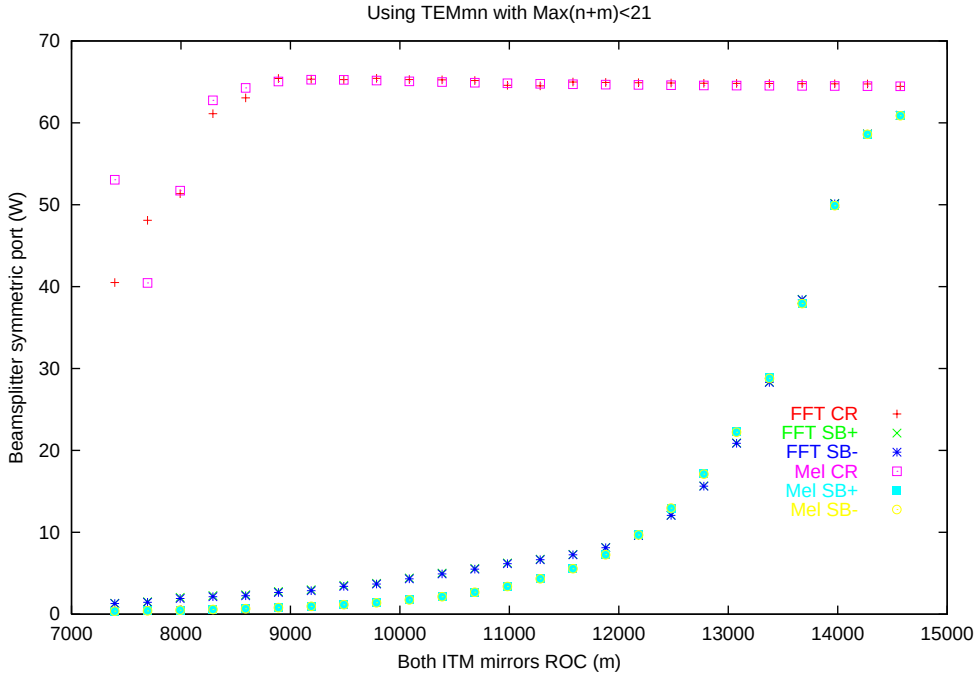

FIG. 6. The deformation of two mirrors is applied symmetrically and it causes a reduction in the overall gain. No imbalance is appreciated between the intensities of the sidebands

Input parameter	FFT input file	Melody input files
Mirrors' shape	diameter, r.o.c., thick.	diameter, r.o.c., height
Optics constants	R_{ref}, $R_{A.R.}$, T, L	R_{ref}, T, L_{ref}, $L_{A.R.}$, L_{bulk}
Laser	carrier and modul. freq.	carrier and modul. freq.
Beam's geometry	spot size and r.o.c.	Max $m+n$ for TEMmn
Materials	refractive index	all the properties

TABLE I. The most important physical parameters driving the simulations

Basic informations	FFT summary file	Melody summary file
Lengths	optimized values	optimized values
Beam amplitude	adapted to mirrors	distorted as mirrors
Round-trip phases	arms, rec. cav.	arms, rec. cav.
Final Power	b.s. ports, arms, refl., RM	b.s. ports, arms, refl.
Decomposition	TEM00, TEM01, TEM10	TEMmn $m+n<N$

TABLE II. Fundamental results collected in the summary output text files

	R.M.	B.S.	$ITM_{on-line}$	$ETM_{on-line}$	$ITM_{off-line}$	$ETM_{off-line}$
r^2	0.98502	0.499975	0.97	0.999935	0.97	0.999935
t^2	0.01493	0.499975	0.02995	0.000015	0.02995	0.000015
L	0.00005	0.00005	0.00005	0.00005	0.00005	0.00005

TABLE III. The input parameters for reflectivity, transmittance and loss

Gains values	FFT-code	Melody	Analytical
Power by rec. mirror	65.6943		65.7331
On-line arm cav.	4288.09	4283.92	4290.62
Off-line arm cav.	4288.09	4283.92	4290.62
B.S. bright port	64.6979	64.6826	64.7365

TABLE IV. Comparison of the numerical results and the mathematical calculations

	R.M.	B.S.	$ITM_{on-line}$	$ETM_{on-line}$	$ITM_{off-line}$	$ETM_{off-line}$
r^2	0.00005	0.5	0.97	0.999935	0.0001	0.00005
t^2	0.9999	0.5	0.02995	0.000015	0.99985	0.000015
L	0.00005	0	0.00005	0.00005	0.00005	0.999935

TABLE V. The parameters that define an asymmetric design of the interferometer

Gains values	FFT-code	Melody	Analytical
Power by rec. mirror	1.00695		1.00693
On-line arm cav.	65.722	65.729	65.729
Off-line arm cav.	0.5035	0.5035	0.5035
B.S. bright port	0.2493	0.2494	0.2465
B.S. dark port	0.2464	0.2465	0.2494

TABLE VI. Gains for an asymmetric interferometer with only one arm on resonance